

Multi-objective Genetic Algorithm Optimization of a Neural Network for Estimating Wind Speed Prediction Intervals

Ronay Ak^a, Yanfu Li^a, Valeria Vitelli^a, Enrico Zio^{a,b,*}

^a*Chair on Systems Science and the Energetic Challenge, European Foundation for New Energy-Electricité de France
École Centrale Paris, Grande Voie des Vignes, Châtenay-Malabry, 92290 France, and SUPELEC, Plateau du Moulon - 3 Rue
Joliot-Curie, Gif-Sur-Yvette, 91192 France*

^b*Department of Energy, Politecnico di Milano, Via Ponzio 34/3 Milan, 20133 Italy*

Abstract — In this work, the non-dominated sorting genetic algorithm-II (NSGA-II) is applied to determine the weights of a neural network trained for short-term forecasting of wind speed. More precisely, the neural network is trained to produce the lower and upper bounds of the prediction intervals of wind speed. The objectives driving the search for the optimal values of the neural network weights are the coverage of the prediction intervals (to be maximized) and the width (to be minimized). A real application is shown with reference to hourly wind speed, temperature, relative humidity and pressure data in the region of Regina, Saskatchewan, Canada. Correlation analysis shows that the wind speed has weak dependence on the above mentioned meteorological parameters; hence, only hourly historical wind speed is used as input to a neural network model trained to provide in output the one-hour-ahead prediction of wind speed. The originality of the work lies in proposing a multi-objective framework for estimating wind speed prediction intervals (PIs), optimal both in terms of accuracy (coverage probability) and efficacy (width). In the case study analyzed, a comparison with two single-objective methods has been done and the results show that the PIs produced by NSGA-II compare well with those and are satisfactory in both objectives of high coverage and small width.

Keywords: wind energy, wind turbine, short-term wind speed forecasting, prediction intervals, neural networks, multi-objective genetic-algorithms.

1. Introduction

Power production via renewable energy sources is a hot topic of research and application. This is due to both the widespread availability of such sources (e.g. wind, sun, etc.) and the sustainability of the production process. Among renewable energy sources, wind currently plays a key role in many countries. As a kind of non-polluting renewable energy, wind power has tremendous potential in commercialization and bulk power generation. According to the Half-Year Report 2011 released by The World Wind Energy Association (WWEA) [1], the worldwide wind capacity reached 215000 MW at the end of June 2011 and the global wind capacity grew of 9.3 % in the previous six months, and 22.9% on an annual basis (mid-2011 compared to mid-2010). According to the 2011 European Statistics Report of the European Wind Energy Association (EWEA) [2], annual wind power installations in the EU have increased steadily over the past 17 years from 814 MW in 1996 to 9616

MW in 2011, an average annual growth rate of 15.6%. This continuous and rapid growth indicates that wind energy represents a popular solution for meeting the increasing need of electricity, respectful of the environment and sustainable.

In a power network, generated power should cover the power demand at any given time. The power output of a wind turbine is mainly dependent on the local wind speed, and the physical and operating characteristics of the turbine. Wind speed changes according to weather conditions, in time scales ranging from minutes to hours, days and years [3]; then, the wind power output also varies. Wind power variations in short-term time scales have significant effects on power system operations such as regulation, load following, balancing, unit commitment and scheduling [3-7]. Thus, accurate prediction of wind speed and its uncertainty is critical for the safe, reliable and economic operation of the power system.

Wind speed and power forecasting have been tackled in the literature by a variety of methods, including numerical weather prediction (NWP) and statistical models (these latter comprising also artificial intelligence methods like neural networks (NN) and fuzzy logic) [3-8]. Hybrid approaches combining physical and statistical models have also been proposed [9, 10]. While physical models are suited for long-term forecasting (predictions for days, weeks and months ahead), statistical and hybrid approaches are the most promising for short-term forecasting (predictions for seconds, minutes and few hours ahead) [3-10]. Among these, NNs are attractive because of their capability of approximating non-linear relationships among multiple variables [4-8].

The existing studies on the use of NN for wind speed prediction aim at providing only point predictions. On the other hand, in practice the accuracy of the point predictions can be significantly affected by the uncertainties in the network structure and input data [11-13], and this is relevant for the design and operation conditions which follow.

Prediction intervals (PIs) can be estimated to provide a measure of the uncertainty in the prediction. PIs are comprised of lower and upper bounds within which the actual target is expected to lie with a predetermined probability [11-13]. There are two competing criteria for assessing the quality of the estimated PIs: coverage probability (CP) and prediction interval width (PIW) [12]. One seeks to simultaneously minimize PIW and maximize CP, which however are conflicting objectives.

In this work, we tackle this problem by adopting a multi-

* Corresponding author at: Chair on Systems Science and the Energetic Challenge, Ecole Central Paris, Châtenay-Malabry, 9220 France. Tel.: +33 (0)1 4113 1606; fax: +33 (0)1 4113 1272.
E-mail address: enrico.zio@ecp.fr (E. Zio).

objective genetic algorithm (MOGA) framework, i.e. non-dominated sorting genetic algorithm-II (NSGA-II) [14], to determine the values of the weights of a NN trained to estimate the bounds defining the prediction intervals. The work extends the Lower and Upper Bound Estimation (LUBE) method of [12], which combines CP and PIW in one single quality measure for optimization. Demonstration of the approach is given in [15] on a synthetic case study of literature. In the present work, a real problem concerning the short-term (1h ahead) wind speed prediction is considered. Wind and other meteorological parameters for the region of Regina, Saskatchewan, Canada have been downloaded from [16]. The data are first analyzed to identify correlations among variables and to help defining the structure of the predictive model.

In the case study analyzed a comparison is also made between the method proposed in this paper, the single objective simulated annealing (SOSA) method of [12], and a single objective genetic algorithm (SOGA).

The paper is organized as follows. Section 2 briefly introduces the basic concepts of NN and PIs, and reviews some existing methods for the construction of NN PIs. In Section 3, basic principles of multi-objective optimization and the NSGA-II method are briefly recalled. Section 4 illustrates the use of NSGA-II for training a NN to estimate PIs. Experimental and comparison results on the real case study of wind speed prediction and are given in Section 5. Finally, Section 6 concludes the paper with a critical analysis of the results obtained and some ideas for future studies.

2. NNs and PIs

Neural networks (NNs) are a class of nonlinear statistical models inspired by brain architecture, capable of learning complex nonlinear relationships among variables from observed data. This is done by a process of parameter tuning called "training".

It is common to represent the task of a NN model as one of nonlinear regression of the kind [17, 18]:

$$y = f(x; w^*) + \varepsilon(x), \quad \varepsilon(x) \sim N(0, \sigma_\varepsilon^2(x)) \quad (1)$$

where x , y are the input and output vectors of the regression, respectively, and w^* represents the vector of values of the parameters of the model function f , in general nonlinear. The term $\varepsilon(x)$ is the error associated with f , and is assumed normally distributed with zero mean. For simplicity of illustration, in the following we assume y one-dimensional. An estimate \hat{w} of w^* can be obtained by a training procedure aimed at minimizing the quadratic error function on a training set of input/output values $D = \{(x_n, y_n), n = 1, 2, \dots, n_p\}$,

$$E(w) = \sum_{i=1}^{n_p} (\hat{y}_i - y_i)^2 \quad (2)$$

where $\hat{y}_i = f(x_i; \hat{w})$ represents the output provided by the NN in correspondence of the input x_i and n_p is the total number of training samples.

Fig. 1 shows the structure of a typical three layer (input, hidden and output) multi-layer perceptron (MLP) neural network. Each layer contains some neurons (nodes). It receives input signals generated by the previous layer, produces output signals through a process and it distributes them to the subsequent layer through the neurons. The nodes are connected by weights and convert input data into values between 0 and 1 by using a sigmoid transfer (activation) function.

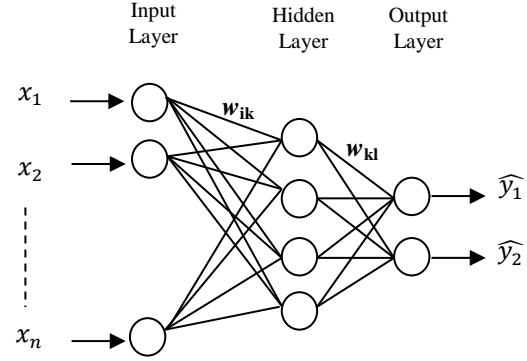


Fig. 1. Architecture of a MLP NN model.

A multiple-input neuron with information processing through this neuron is illustrated in Fig. 2. The output signal H of node j of the hidden layer is given by [19-22]:

$$H_j = f_{act(net_j)} = f_h(w_{0j}b_j + \sum_{i=1}^{n_p} w_{ij}x_i) \quad (3)$$

where $j = 1, 2, \dots, h$ and h indicates the number of hidden neurons, w_{ij} is the synaptic weight, $f_{act(net_j)}$ is the activation or transfer function and b_j is a bias factor taken as 1. After each hidden neuron computes its activation, it sends its signal to each of the neurons o_l in the output layer. Each output neuron o_l computes its output signal O_l to form the response of the net for the input pattern [23]:

$$O_l = f_o(w_{0l}b_l + \sum_{j=1}^h w_{jl}H_j) \quad l = 1, 2, \dots, n_o \quad (4)$$

where n_o is the number of output neurons, and f_o indicates the activation function used in the output layer.

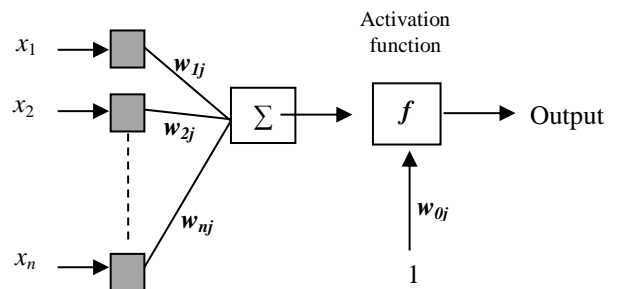


Fig. 2. Multiple input neuron [21].

A PI is defined by upper and lower bounds that include a future unknown value with a predetermined probability, called confidence level $(1 - \alpha)$. The formal definition of a PI is the following:

$$\Pr(L(x) < y(x) < U(x)) = 1 - \alpha \quad (5)$$

where $L(x)$ and $U(x)$ are respectively the lower and upper bounds of the PI of the output $y(x)$ corresponding to input x ; the confidence level $(1 - \alpha)$ refers to the expected probability that the true value of $y(x)$ lies within the PI $(L(x), U(x))$.

The main reason for estimating the PI of the NN model output comes from the need of accounting for both the uncertainty in the model structure and the noise in the input data, which affect the point estimates. Two measures are used to evaluate the quality of the PIs: the coverage probability (CP) and the interval width (IW) [11-13]. The prediction interval coverage probability (PICP) represents the probability that the set of estimated PIs will contain the true output values, estimated as the proportion of true output values lying within the estimated PIs; the prediction interval width (PIW) simply measures the extension of the interval as the difference of the estimated upper bound and lower bound values. These are in general conflicting measures (wider intervals give larger coverage), and in practice it is important to have narrow PIs with high coverage probability [12].

Techniques for estimating PIs for NN model outputs are the Delta, Bayesian, Mean-variance estimation (MVE) and Bootstrap techniques [11]. The Delta method is based on a Taylor expansion of the regression function. This method is capable of generating high quality PIs but at the cost of high computational time in the development stage, because it requires the calculation of a Jacobian matrix and the unbiased estimation of the noise variance [11, 24].

The Bayesian approach uses a Bayesian statistics approach to express the uncertainty of the neural network parameters in terms of probability distributions, and integrates these to obtain the posterior probability distribution of the target conditional on the observed training set [24-26]. The underpinning axiomatic mathematical foundation makes this method robust and highly repeatable. In the end, NNs trained by a Bayesian-based learning technique have superior generalization power [11]. On the other hand, the computation time required is high, due to the calculation of a Hessian matrix in the development stage (a situation similar to the Delta technique).

MVE estimates the mean and the variance of the probability distribution of the target as a function of the input, given an assumed target error distribution model [27]. The proposed model is based on the maximum-likelihood formulation of a feed-forward NN [27]. Compared to the aforementioned techniques, the computational burden of this method is negligible both in the development and PI estimation stages. However, the method underestimates the variance of the data, so that the quality and generalization

power of the PIs obtained are low [11, 12].

The Bootstrap method is frequently used because it is the simplest method among the ones mentioned here. It is a re-sampling technique that allows assigning measures of accuracy to statistical estimates and does not require the calculation of complex matrices and derivatives [24, 28]. The aim of the re-sampling is to produce less biased estimates of the true regression of the targets and improve the generalization performance of the model [11]. Main disadvantages are: i) high computational time when the training sets and neural networks are large; ii) with small numbers of input patterns, the individual neural networks tend to be overly trained, leading to poor generalization performance [11, 17].

The common feature of the above PI estimation methods is that they do not take into account the widths of the intervals [11]. With respect to this point, Khosravi et. al. [12] proposed a ‘‘Lower and Upper Bound Estimation Method (LUBE)’’ in which the cost function in Eq. (8) to be minimized combines two quantitative measures: PICP and PIW. The mathematical definition of the PICP and PIW measures used are [12]:

$$PICP = \frac{1}{n_p} \sum_{i=1}^{n_p} c_i \quad (6)$$

where n_p is the number of samples in the training or testing sets, and $c_i = 1$, if $y_i \in [L(x_i), U(x_i)]$ and otherwise $c_i = 0$,

$$NMPIW = \frac{1}{n_p} \sum_{i=1}^{n_p} \frac{(U(x_i) - L(x_i))}{t_{max} - t_{min}} \quad (7)$$

where $NMPIW$ is the Normalized Mean PIW, and t_{min} and t_{max} represent the true minimum and maximum values of the targets (i.e., the bounds of the range in which the true values fall) in the training set, respectively. Normalization of the PI width by the range of targets makes it possible to objectively compare the PIs, regardless of the techniques used for their estimation or the magnitudes of the true targets.

The cost function proposed in [12] is called coverage width-based criterion (CWC):

$$CWC = NMPIW(1 + \gamma(PICP) e^{-\eta(PICP - \mu)}) \quad (8)$$

where η and μ are constants. The role of η is to magnify any small difference between μ and PICP. The value of μ gives the nominal confidence level, which is set to 90% in our experiments. Then, η and μ are two parameters determining how much penalty is paid by the PIs with low coverage probability. The function $\gamma(PICP)$ is equal to 1 during training, whereas in the testing of the NN it is given by the following step function:

$$\gamma(PICP) = \begin{cases} 0, & PICP \geq \mu \\ 1, & PICP < \mu \end{cases} \quad (9)$$

In Fig. 3, a symbolic sketch of the proposed NN model with two outputs is illustrated. The first output neuron

provides the upper bound and the second the lower bound. With these two output neurons, the NN generates a PI interval for each input pattern.

Notice that, the LUBE method directly provides in output the PIs while the previously described methods do so in two steps (first, point estimate calculation and then, PIs estimation).

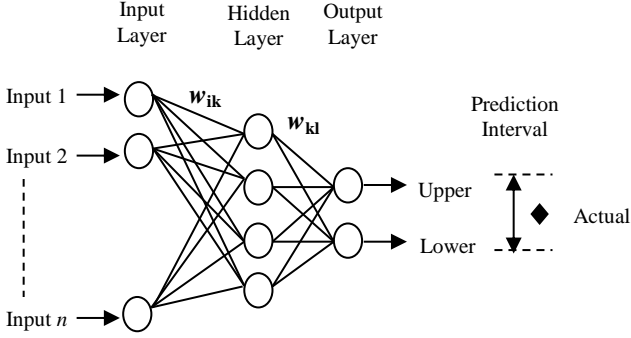


Fig. 3. Architecture of a Multi-layer feed forward NN model for estimating the lower and upper bounds of PIs [12].

3. Multi-objective optimization by NSGA-II

In all generality, a multi-objective optimization problem consists of a number of objectives and is associated with a number of equality and inequality constraints, and bounds on the decision variables. Mathematically the problem can be written as follows [29]:

$$\text{Minimise/Maximise } f_m(x), \quad m = 1, 2, \dots, M; \quad (10)$$

$$\text{subject to } g_j(x) \geq 0, \quad j = 1, 2, \dots, J; \quad (11)$$

$$h_k(x) = 0, \quad k = 1, 2, \dots, K; \quad (12)$$

$$x_i^{(l)} \leq x_i \leq x_i^{(u)} \quad i = 1, 2, \dots, I. \quad (13)$$

A solution, $x = \{x_1, x_2, \dots, x_I\}$ is an I dimensional decision variable vector in the solution space R^I . The solution space is restricted by the constraints in (11) and (12) and bounds on the decision variables in (13).

The M objective functions $f_m(x)$ must be evaluated in correspondence of each decision variable vector x in the search space. The final goal is to identify a set of optimal solutions $x^* \in R^I$ in which no solution can be regarded as better than any other with respect to all the objective functions. The comparison of solutions may be performed in terms of the concepts of Pareto optimality and dominance: in case of a minimization problem, solution x_a is regarded to dominate solution x_b ($x_a > x_b$) if both following conditions are satisfied [29]:

$$\forall i \in \{1, 2, \dots, M\}, f_i(x_a) \leq f_i(x_b) \quad (14)$$

$$\exists j \in \{1, 2, \dots, M\}, f_j(x_a) < f_j(x_b) \quad (15)$$

If any of the above two conditions is violated, the solution x_a does not dominate the solution x_b , and x_b is said to be non-dominated by x_a . The solutions that are non-dominated within the entire search space are denoted as Pareto-optimal and constitute the Pareto-optimal set; the corresponding values of the objective functions form the so called Pareto-optimal front in the objective functions space. The goal of a multi-objective optimization algorithm is to guide the search for solutions in the Pareto-optimal set, while maintaining diversity so as to cover well the Pareto-optimal front and thus allow flexibility in the final decision on the solutions to be actually implemented. The Pareto optimal set of solutions can provide the decision makers (DMs) the flexibility to select the appropriate solutions with different preferences on the objectives. The decision makers also gain insights into the characteristics of the optimization problem before a final decision is made.

Genetic algorithm (GA) is a popular meta-heuristic approach well-suited for multi-objective problems [30]. It is a population based-search technique inspired by the principles of genetics and natural selection. Multi-objective GAs (MOGAs) are frequently applied for solving the multi-objective optimization problems, for their ability to find nearly global optima, the ease of use and the robustness [31-33].

Among the several variations of MOGA in the literature, we select non-dominated Sorting Genetic Algorithm-II (NSGA-II) as the optimization tool, because the comparative studies [14, 30, 31] have shown that it is one of the most efficient MOGAs.

4. Implementation of NSGA-II for training a NN for estimating PIs

In this work, we adapt the LUBE method [12] to the multi-objective formulation of the PI estimation problem. More specifically, we use NSGA-II for finding the values of the parameters of the NN which minimize the two objective functions PICP (6) and NMPIW (7) simultaneously, in Pareto optimality sense (for ease of implementation, the maximization of PICP is converted to minimization by subtracting from one, i.e. the objective of the minimization is 1-PICP).

The practical implementation of NSGA-II on our specific problem involves two phases: initialization and evolution. These can be summarized as follows (see Fig. 4):

Initialization phase:

Step 1: Split the input data into training (D_{train}) and testing (D_{test}) subsets.

Step 2: Fix the maximum number of generations and the number of chromosomes (individuals) Nc in each population; each chromosome codes a solution by G real-valued genes, where G is the total number of parameters (weights) in the NN. Set the generation number $n = 1$. Initialize the first population P_n of size Nc , by randomly generating Nc chromosomes.

Step 3: For each input vector x in the training set, compute

the lower and upper bound outputs of the Nc NNs, each one with G parameters.

Step 4: Evaluate the two objectives PICP and NMPIW for the Nc NNs (one pair of values 1-PICP and NMPIW for each of the Nc chromosomes in the population P_n).

Step 5: Rank the chromosomes (vectors of G values) in the population P_n by running the fast non-dominated sorting algorithm [14] with respect to the pairs of objective values, and identify the ranked non-dominated fronts F_1, F_2, \dots, F_k where F_1 is the best front, F_2 is the second best front and F_k is the least good front.

Step 6: Apply to P_n a binary tournament selection based on the crowding distance [14], for generating an intermediate population S_n of size Nc .

Step 7: Apply the crossover and mutation operators to S_n , to create the offspring population Q_n of size Nc .

Step 8: Apply *Step 3* onto Q_n and obtain the lower and upper bound outputs.

Step 9: Evaluate the two objectives in correspondence of the solutions in Q_n , as in *Step 4*.

Evolution phase:

Step 10: If the maximum number of generations is reached, stop and return P_n . Select the first Pareto front F_1 as the optimal solution set. Otherwise, go to *Step 11*.

Step 11: Combine P_n and Q_n to obtain a union population $R_n = P_n \cup Q_n$.

Step 12: Apply *Steps 3-5* onto R_n and obtain a sorted union population.

Step 13: Select the Nc best solutions from the sorted union to create the next parent population P_{n+1} .

Step 14: Apply *Steps 6-9* onto P_{n+1} to obtain Q_{n+1} . Set $n = n + 1$; and go to *Step 10*.

Finally, the best front in terms of ranking of non-dominance and diversity of the individual solutions is chosen. Once the best front is chosen, then the testing step is performed on the trained NN with optimal weight values.

GA uses two operators to generate new solutions from existing ones: crossover (recombination) and mutation (see *step 7*).

Crossover is the key operator for the effectiveness of GA, and it is used to create two new chromosomes called offsprings from one selected pair of chromosomes called parents. We have used extended intermediate recombination method as a crossover operator [34]. Intermediate recombination can produce any point within a hypercube slightly larger than that defined by the parents [34] and it can only be applied to real-coded GAs [35]. Offsprings are produced as follows:

- Randomly select the crossover point (position) $j \in \{1, \dots, S\}$.

- Randomly select the parents $P_1 = (p_1^1, \dots, p_S^1)$ and $P_2 = (p_1^2, \dots, p_S^2)$ depending on the crossover probability.

- Set $C_1 = P_1$ and $C_2 = P_2$. Then, in order to create two offsprings $C_1 = (c_1^1, c_2^1, \dots, c_j^1, c_{j+1}^1, \dots, c_S^1)$ and $C_2 = (c_1^2, c_2^2, \dots, c_j^2, c_{j+1}^2, \dots, c_S^2)$, change the genes from j to S according to the following procedure:

$$(c_j^1, c_{j+1}^1, \dots, c_S^1) = (p_j^1, p_{j+1}^1, \dots, p_S^1) + r_1 * [(p_j^2, p_{j+1}^2, \dots, p_S^2) - (p_j^1, p_{j+1}^1, \dots, p_S^1)] \quad (16)$$

$$(c_j^2, c_{j+1}^2, \dots, c_S^2) = (p_j^1, p_{j+1}^1, \dots, p_S^1) + r_2 * [(p_j^2, p_{j+1}^2, \dots, p_S^2) - (p_j^1, p_{j+1}^1, \dots, p_S^1)] \quad (17)$$

where r_1 and r_2 are two values randomly (uniformly) chosen within the interval $[-0.25, 1.25]$ [35].

Mutation involves the modification of the value of each gene of a solution with a predefined probability P_m (the mutation rate) [36]. For performing mutation, we have used a heuristic method, similar to non-uniform mutation [37], where the mutation probability (rate) P_m decreases at each generation. In our mutation method, the selected gene is replaced with a new real coded value generated by the following algorithm:

$$c_j^i = c_j^i + (rand - 0.5) * 2 \quad i = 1, \dots, Nc \text{ and } j = 1, \dots, S \quad (18)$$

where i and j indicate the chromosome and the gene within the chromosome to be mutated, respectively, Nc is the number of chromosomes, and $rand$ indicates a random number value drawn from the standard uniform distribution on the open interval $(0,1)$.

The total computational complexity of the proposed algorithm can be explained by two time demanding sub-operations: nondominated sorting and fitness evaluation. The time complexity of nondominated sorting part is $O(MNc^2)$ where M shows the number of objectives and Nc shows the population size [14]. In fitness evaluation phase, the NSGA-II has been used to train a NN which has n_p input samples. Since for each individual of the population a fitness values is obtained, this process is repeated $Nc \cdot n_p$ times. Hence, time complexity of this phase is $O(Nc \cdot n_p)$. In conclusion, the computation complexity of one generation is $O(MN^2 + Nc \cdot n_p)$.

5. Experiments and results

In this Section, results of the application of the proposed method to short-term wind speed forecasting are detailed. The considered wind speed data have been measured in Regina, Saskatchewan, a region of central Canada. Wind farms in Canada are currently responsible of an energy production of 5403 MW, a capacity big enough to power over 1 million homes and equivalent to about 2% of the total electricity demand in Canada [38]. The actual situation in Saskatchewan is characterized by the presence of 4 large wind farms located throughout the region, with a total capacity of approximately 198 MW. Aside from large wind farms, Saskatchewan residents have installed numerous smaller wind turbines (approximately 200), most of which characterized by a power production of less than 10 KW [39].

5.1. Pre-treatment of input data

The hourly wind speeds measured in Regina,

Saskatchewan, in two different periods of the year, from 1st of February 2012 to 31st of March 2012 and from 1st of July 2012 to 29th of August 2012 have been downloaded from the website [16]. In addition to the hourly wind speed data, the hourly measurements concerning three meteorological variables (temperature, relative humidity and air pressure) are also available for the same area in the same time periods.

In order to have insights on the strength of the relationship between the input variables (the meteorological explanatory variables) and the output variable (wind speed), some statistical analyses of the data have been conducted. First, the correlation structure of the data matrix has been explored through various correlation indexes and statistical tests [40]. The results obtained by computing Pearson's correlation coefficient are reported in Table 1, and they show that wind speed has in fact weak (lower than 40%) dependences on the meteorological parameters considered, both during summer and during winter. We also performed two different non-parametric tests of no correlation, based on Kendall's τ and Spearman's ρ statistics [41]: both statistical tests give strong evidence of absence of correlation between wind speed and all meteorological variables, both during summer and winter (p -values all below 10-10). Finally, also the correlations among meteorological variables have been explored by all these means, and they all resulted to be negligible.

Table 1
Correlation matrix for the explanatory and output variables (winter/summer).

	Temp.	Wind speed	Relative hum.	Air pres.
Temp.	1			
Wind speed	0.362/0.140	1		
Relative hum.	-0,506/ -0,758	-0.269/-0.203	1	
Air pres.	-0,591/ -0,098	-0.282/-0.333	0.129/-0,037	1

Secondly, a Principal Component Analysis (PCA) of the meteorological variables was performed using the correlation matrix shown in Table 1 (without the output variable, wind speed). Indeed, when principal components loadings, i.e. the weights in the combinations defining the components, are interpretable and physically meaningful, a possibility is to use as explanatory variables in the model the projections of the original input variables on the principal component space [42]. In this way, the new input variables for the model are less correlated among each other, and possibly more correlated to the target. However, results of PCA (see Table 2) show not so neat and interpretable loadings. Moreover, the new variables obtained by projection of the explanatory input variables on the first two principal components (which together explain more than 90% of the total variability in the dataset, see the last row of Table 2), do not show an increase in the correlation with the target: $\rho(wind, PC1) = 36.21\%$ in winter and 19.83% in summer; $\rho(wind, PC2) = 24.88\%$ in winter and 13.03% in summer.

All previous considerations support the conclusion that

the influence of meteorological variables on the observed wind speed and their mutual dependence, are not a sufficient motivation for including them in the model as explanatory variables. This is not surprising: many models for describing wind condition or wind speed proposed in the literature rely only on past wind speed data [43], or other information concerning wind (e.g. wind direction) [44]. Hence, only historical wind speed values are selected as input variables for the ANN model aimed at providing in output the one-hour-ahead prediction of wind speed.

Table 2
Results of the PCA on meteorological variables (winter/summer).

	1 st Principal component loadings	2 nd Principal component loadings	3 rd Principal component loadings
Temp.	0.677/0.708	--/--	0.735/-0.704
Relative hum.	-0.49/-0.703	-0.762/-0.128	0.423/-0.699
Air pres.	-0.549/--	0.647/0.991	0.53/-0.124
Proportion of explained variance	0.615/0.587	0.291/0.336	0.094/0.076
Cumulative proportion of explained variance	0.615/0.587	0.906 /0.924	1/1

The last choice concerning the model inputs for the NN model is the number of the past wind speed values to consider. First, the analysis of the empirical Autocorrelation Function (ACF; Fig. 5, top, left for winter and right for summer) shows a non-negligible correlation of the wind speed time series, also for high values of the lag. Typically in time series analysis such a consideration leads to the fitting of an autoregressive model, which explains the current value of the target via a linear combination of past values of the target itself [45]. Even if NNs are nonlinear models, this fact can be taken as an indication of the relevance of the past values of the wind (W_{t-1}, \dots, W_{t-k}) to explain the current wind speed (W_t). The empirical Partial Autocorrelation Function (PACF; Fig. 5, bottom, left for winter and right for summer) is instead commonly used in time series analysis for model identification, i.e. for the choice of k [45]: specifically, PACF at lag j is the autocorrelation between W_t and W_{t-j} that is not accounted for by lags 1 through $j-1$, and in autoregressive models of order k the PACF is zero at lag $k + 1$ or greater. We thus look for the point on the plot where the PACF essentially becomes zero, and detect the lags at which PACF is not significantly different from zero by a 95% Confidence Interval (CI), whose limits are at $\pm Z_{0.975} / \sqrt{n}$, where n is the dimension of the dataset. The CI limits correspond to the dotted lines in Fig. 5 (bottom): we can see that W_{t-1} and W_{t-2} are highly correlated to W_t , and hence should be used in the prediction, both for the winter and the summer season; indeed, for the winter time series, also W_{t-3} is significantly related to W_t , and should thus be used in the prediction model. In synthesis, historical wind speed values W_{t-1}, W_{t-2} and W_{t-3} are selected as input variables for predicting W_t in output for the winter season, while during summer only W_{t-1} and W_{t-2} are selected as inputs.

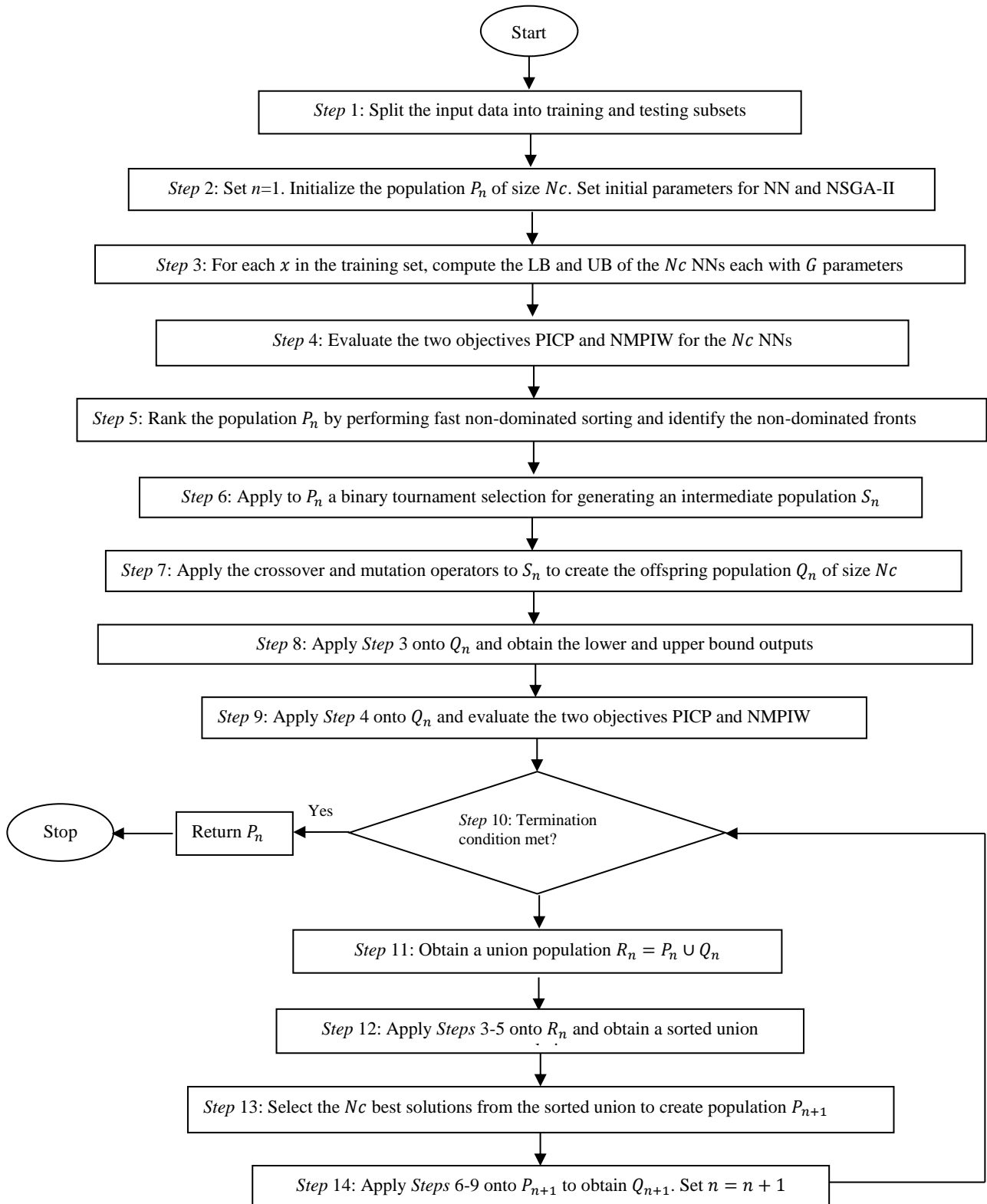


Fig. 4. A framework for the NSGA-II method used for training of NNs for PI estimation.

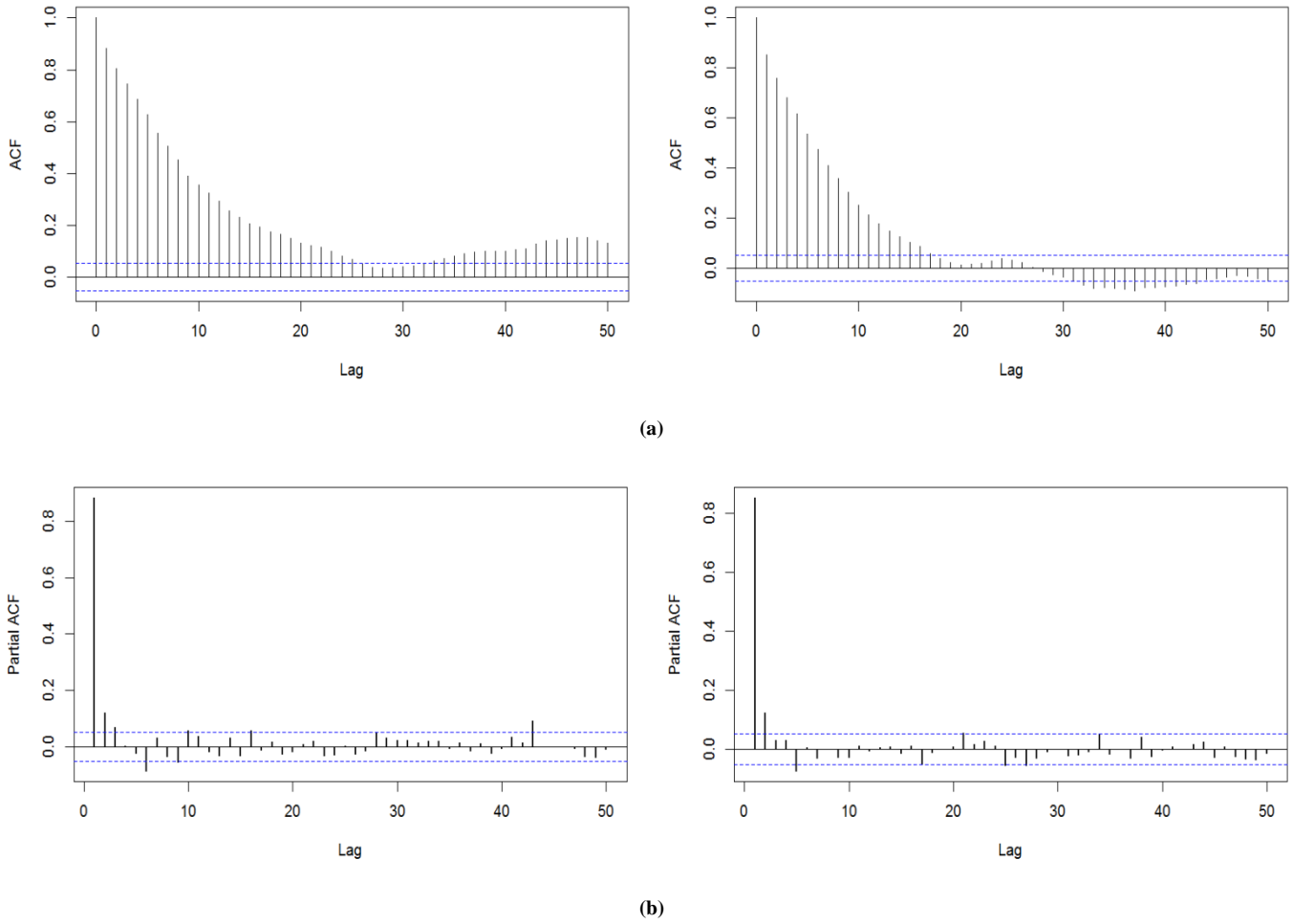


Fig. 5. (a) ACF plot for the wind speed time series: winter (left) and summer (right).
 (b) PACF plot for the wind speed time series: winter (left) and summer (right).

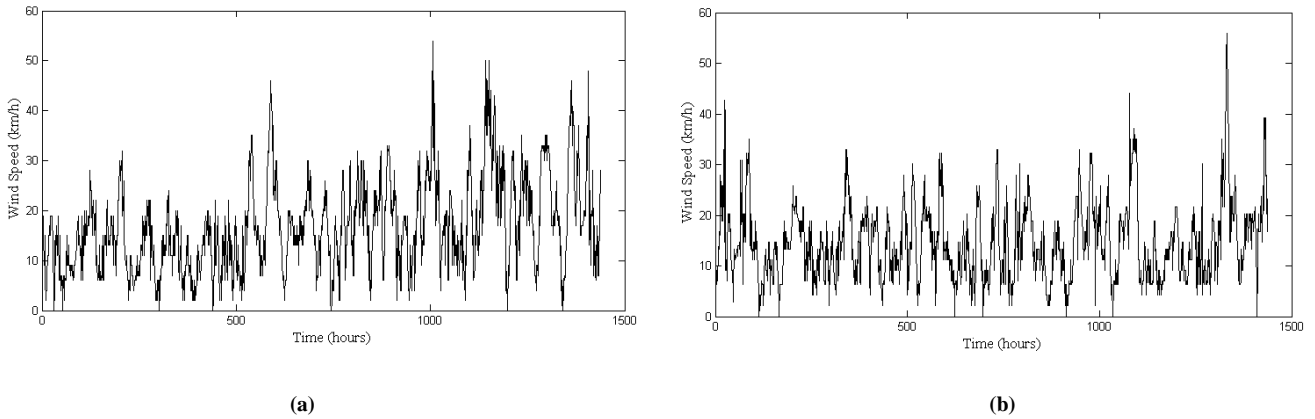


Fig. 6. The wind speed data set used in this study: (a) winter period (b) summer period.

5.2. NN Training and testing results

The first data set (winter period) includes 1437 samples (see Fig. 6), among which the first 80% (the first 1150 samples) is used for training and the rest for testing. The second data set (summer period) includes 1438 samples (see

Fig. 6), among which the first 80% (the first 1150 samples) is used for training and the rest for testing.

The architecture of the NN consists of one input, one hidden and one output layers. The number of input neurons is set to 2 for summer data and to 3 for winter data; the number

of hidden neurons is set to 10 after a trial-and-error process; the number of output neurons is 2, one for the lower and one for the upper bound values of the PIs. As activation functions, the hyperbolic tangent function is used in the hidden layer and the logarithmic sigmoid function is used at the output layer (these choices have been found to give the best results by trial and error, although the results have not shown a strong sensitivity to them).

For the first case study (winter period), the inputs to the input neurons are the wind speed values of the previous three time steps (W_{t-1} , W_{t-2} and W_{t-3}). For the second one (summer period), the previous two time steps (W_{t-1} and W_{t-2}) have been used as inputs. All data have been normalized within the range [0.1, 0.9].

Table 3 contains the parameters of the NSGA-II for training the NN. “MaxGen” indicates the maximum number of generations which is used as a termination condition and Nc indicates the total number of individuals per population. P_{m_int} is the initial mutation probability and it decreases at each iteration (generation) by the formula:

$$P_{m_int} \times e^{\left(-\frac{gen}{MaxGen}\right)}. P_c \text{ indicates the crossover probability and is fixed during the run.}$$

Table 3
Parameters used in the experiments.

Parameter	Numerical value
D (input pattern set)	1438 (winter data) 1437 (summer data)
$D_{training}$ (training set)	1150 (winter data) 1150 (summer data)
$D_{testing}$ (testing set)	288 (winter data) 287 (summer data)
MaxGen	300
Nc	50
P_{m_int}	0.06
P_c	0.8
μ	0.9
η	50
T_{init}	5
T_{min}	10^{-50}
CWC_{int}	10^{80}
Geometric cooling schedule of SA	$T_{k+1} = T_k * 0.95$

To account for the inherent randomness of NSGA-II, twenty different runs have been performed and an overall best non-dominated Pareto front has been obtained from the twenty individual fronts. To construct such front, the first (best) front of each of twenty runs is collected and the resulting set of solutions is subjected to the fast non-dominated sorting algorithm [14] with respect to the two objective functions values. Then, the ranked non-dominated fronts F_1, F_2, \dots, F_k are identified, where F_1 is the best front, F_2 is the second best front and F_k is the worst front. Solutions in the first (best) front F_1 are then retained as overall best front solutions. Fig. 7 illustrates the overall best front solutions

obtained with this procedure from the 20 NSGA-II runs both for winter and summer periods.

Given the overall best Pareto set of optimal solutions (i.e. optimal NN weights), one has to pick one (i.e. one trained NN) for use. Two different selection procedures are here employed for choosing a solution, with reference to the Pareto-optimal front of Fig. 7. First, a solution which results in the smallest CWC (see [12] and Eq. 8) is chosen. As a second procedure, the “min-max” method has been used [46]. Table 4 reports the PICP and NMPIW values of the Pareto front solutions both for the training and testing, according to those two different selection methods. The solutions are also marked on the Pareto front of Fig. 7.

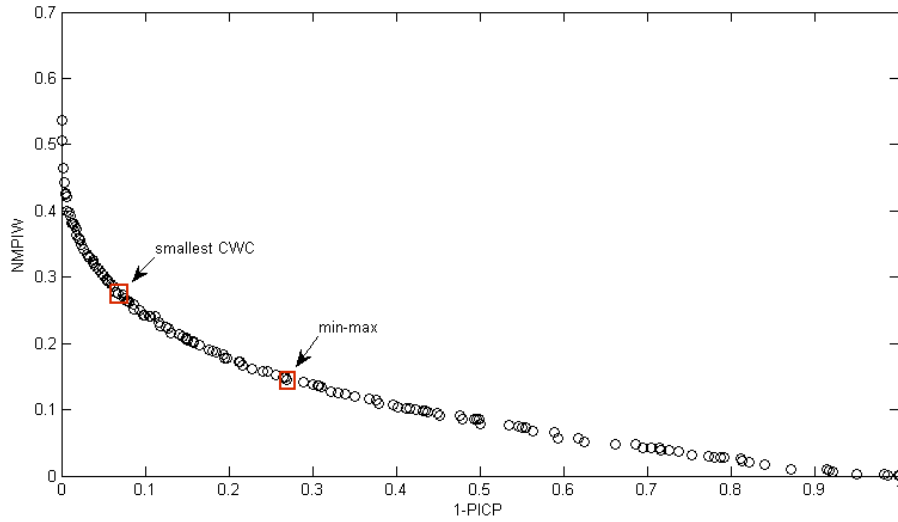
It is observed that the min-max method selects a solution located towards the center of the Pareto-front (see Fig. 7), whereas the smallest CWC selection method gives a solution which has higher coverage probability with larger interval size (see Table 4). This second selection procedure is thus preferable for engineering reasons.

The optimal values of the NN parameters (weights) obtained in training are used for testing on the last 287 and 288 measurements of the wind speed winter and summer data sets, respectively. Figs. 8 and 9 show the prediction intervals for the testing sets of summer and winter, respectively, estimated by the trained NN corresponding to the Pareto solution resulting in the smallest CWC value. The results give a coverage probability of 84% and an average interval width of 0.277 for the winter period, and a coverage probability of 91.7% and an average interval width of 0.326 for the summer period (see Table 4).

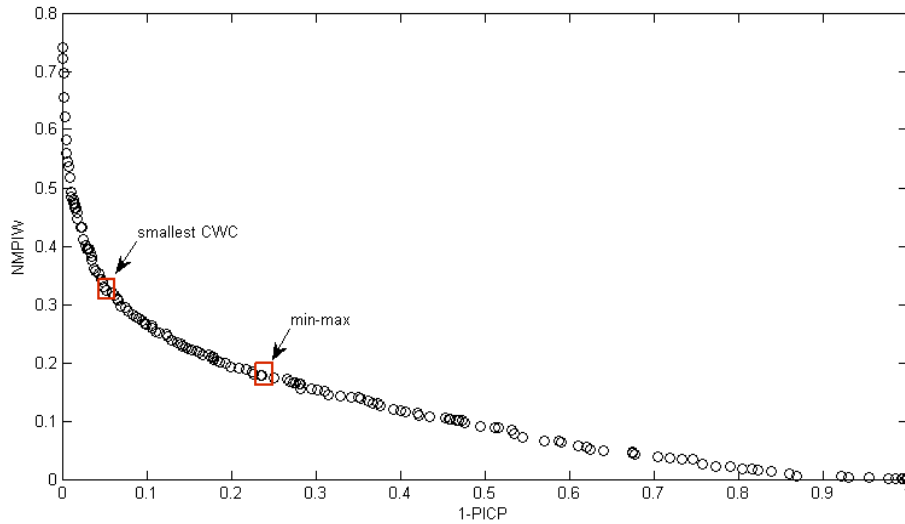
5.3. MOGA comparison with SOSA and SOGA

The single objective genetic algorithm (SOGA) and the single objective simulated annealing (SOSA) procedures, described in [12], have been implemented for comparison. Table 3 also contains the parameters of the experiments run for SOSA and SOGA, together with the parameter for our NSGA-II implementation of the MOGA. The “ T_{init} ”, “ T_{min} ”, “Geometric cooling schedule” and “ CWC_{int} ” are the parameters of the SA optimization technique. “ T_{init} ” and “ T_{min} ” represent the starting and finishing temperatures, respectively. The finishing temperature can be used as a termination condition. The geometric cooling schedule sets the decrease of the temperature at each search iteration [12], [47, 48]. Here, we have used a cooling factor of 0.95. CWC_{int} represents the initial value of the CWC: as the temperature drops during the search, the CWC value decreases gradually but not monotonically [12].

In the MOGA and SOGA, the population size is set to 50 and the number of generations to 300, for a total number of evaluations equal to 15000. For fair comparison, SOSA is configured to have equal number of evaluations: therefore, the maximum number of iterations is set to 15000 as termination condition.



(a)



(b)

Fig. 7. The overall best Pareto front obtained by training of the NN for 1h-ahead wind speed prediction: (a) winter period (b) summer period.

Table 4

Solutions chosen from the overall Pareto optimal front of Fig. 7.

Methods	Winter Period				Summer Period			
	Training		Testing		Training		Testing	
	PICP (%)	NMPIW	PICP (%)	NMPIW	PICP (%)	NMPIW	PICP (%)	NMPIW
Smallest_CWC	93.6	0.276	0.84	0.277	94.8	0.323	91.7	0.326
Min_Max	73	0.145	65.5	0.144	76.4	0.177	74	0.175

As mentioned before, to account for the intrinsic randomness present in the SOSA, SOGA and MOGA optimization procedures, all have been run twenty times. In SOSA and SOGA, the CWC has been used as a cost function. For each of the first (best) front found by twenty MOGA runs, a CWC value has been a posteriori calculated by combining the individual PICP and NMPIW values. Then, for each Pareto front, the solution with smallest (best) CWC value is selected among all solutions in the front. This allows

obtaining twenty best CWC values, one selected from each Pareto front. After training, we perform the testing of the trained NNs with fixed optimal parameter values (weights and biases). For each solution obtained from training, corresponding CWC values have been also calculated for testing data set by following the same procedure explained above. Tables 5 and 6 report the CWC values obtained on the testing set of winter and summer, respectively, in each of the 20 runs.

Table 5
Results of twenty SOSA and SOGA runs and twenty best MOGA for NN testing (winter data set).

SOSA			MOGA			SOGA		
CWC	PICP	NMPIW	CWC	PICP	NMPIW	CWC	PICP	NMPIW
0,560	0,906	0,560	0,341	0,920	0,341	0,878	0,889	0,316
0,600	0,902	0,600	0,714	0,899	0,348	0,889	0,889	0,320
0,620	0,923	0,620	0,778	0,892	0,312	1,170	0,882	0,333
0,696	0,913	0,696	0,845	0,892	0,339	1,404	0,878	0,351
0,701	0,927	0,701	0,931	0,889	0,335	1,411	0,875	0,309
0,803	0,979	0,803	1,076	0,882	0,306	1,447	0,875	0,317
0,809	0,979	0,809	1,098	0,885	0,353	1,725	0,871	0,329
0,834	0,976	0,834	1,139	0,882	0,324	1,925	0,868	0,318
0,852	0,930	0,852	1,182	0,882	0,336	2,496	0,861	0,306
1,190	0,899	0,579	1,525	0,875	0,334	2,557	0,861	0,313
2,332	0,875	0,511	1,682	0,871	0,321	2,579	0,861	0,316
5,286	0,847	0,344	2,260	0,864	0,322	2,883	0,857	0,303
8,389	0,857	0,881	2,494	0,861	0,306	3,137	0,857	0,329
8,665	0,833	0,290	2,570	0,861	0,315	4,031	0,850	0,308
37,073	0,819	0,629	2,974	0,857	0,312	4,616	0,847	0,300
53,131	0,812	0,640	4,358	0,847	0,283	6,402	0,840	0,300
144,893	0,780	0,367	5,924	0,840	0,277	6,617	0,840	0,310
525,279	0,760	0,469	6,013	0,840	0,281	7,632	0,836	0,302
7.6968e+04	0,662	0,523	6,270	0,840	0,293	9,119	0,833	0,305
4.1655e+07	0,533	0,449	7,597	0,836	0,301	10,294	0,829	0,291

In order to perform a quantitative comparison for the results obtained with SOSA, SOGA and MOGA, we use a Kruskal-Wallis rank sum test [41]. The Kruskal-Wallis rank sum test is a non-parametric version of the ANOVA [49], and it has the purpose of testing the null hypothesis that the location parameters of the distribution of the variable of interest (CWC in our case) are the same in each group (given by the different procedures). The alternative is that they differ in at least one of the groups. For the purpose of comparison, we take into account the results of all the 20 runs of the three different procedures, on the testing sets of both winter and summer (see Tables 7 and 8). Considering the winter dataset (Table 7), the Kruskal-Wallis test gives no evidence of a difference in the performance (CWC values) among MOGA, SOSA and SOGA (p-value = 35.44%). However, a difference among the procedures can be detected in terms of the final values of NMPIW (p-value = $1.04 \cdot 10^{-7}$). Hence, a Mann-Whitney non-parametric statistical test [50] has been used to perform pairwise comparisons among the procedures, leading to a demonstrated superiority of SOGA (p-value = $6.86 \cdot 10^{-7}$) and MOGA (p-value = $5.22 \cdot 10^{-7}$) over SOSA. Considering the summer dataset (Table 8), instead, a difference among the procedures can be detected in terms of the final values of CWC (p-value = 0.0005754). Analogously, to what has been

done for the winter data set, a Mann-Whitney non-parametric statistical test has been used to perform pairwise comparisons among the three procedures, again resulting in the superiority of SOGA (p-value = 0.001216) and MOGA (p-value = 0.0006094) over SOSA. As for the comparison of SOGA and MOGA, their results always proved to be comparable both in terms of CWC and of NMPIW, for both winter and summer data sets.

Finally, we have analyzed the convergence of CWC along the iterations of the NN training procedure. The behavior of CWC as a function of the iterations is shown in Figs. 10 and 11 for SOSA and SOGA methods, respectively. Since the CWC takes extreme values in the first iterations of SOSA, the logarithm of CWC has been plotted in Fig.10. In the case of SOSA, the CWC decreases gradually but non-monotonically due to the structure of the simulated annealing algorithm. In order to show clearly the convergence and non-monotonicity of the SOSA method, a zoom on the behavior of CWC has been also plotted: the upper plots in Fig. 10 show the values of CWC for the first 500 iterations. On the contrary, from inspection of Fig.11 it is clear that CWC decreases gradually and monotonically in the case of SOGA.

Figs. 12 and 13 show the convergence behavior of PICP and NMPIW through the iterations of the MOGA method for

the winter and summer datasets, respectively. To obtain these graphs, we have considered the two objectives separately (as if they were two single objectives, even if our research does not really focus on the single-objective solutions), and we have selected the extreme solutions on the front obtained at each iteration. In other words, the solution giving maximum

PICP and the one giving minimum NMPIW were selected separately. The motivation behind these last convergence plots is to show the MOGA algorithm's ability to converge, after a certain number of iterations, to the true optimum, which means respectively 100% PICP and 0 NMPIW. This happens for both the single objectives.

Table 6
Results of twenty SOSA and SOGA runs and twenty best MOGA for NN testing (summer data set).

SOSA			MOGA			SOGA		
CWC	PICP	NMPIW	CWC	PICP	NMPIW	CWC	PICP	NMPIW
0,328	0,913	0,328	0,325	0,917	0,325	0,317	0,906	0,317
0,329	0,910	0,329	0,326	0,917	0,326	0,319	0,903	0,319
0,349	0,920	0,349	0,327	0,906	0,327	0,320	0,903	0,320
0,460	0,931	0,460	0,333	0,913	0,333	0,321	0,910	0,321
0,496	0,934	0,496	0,335	0,910	0,335	0,325	0,910	0,325
0,505	0,906	0,505	0,337	0,917	0,337	0,328	0,910	0,328
0,635	0,934	0,635	0,337	0,917	0,337	0,328	0,903	0,328
0,641	0,934	0,641	0,337	0,924	0,337	0,329	0,910	0,329
0,641	0,948	0,641	0,340	0,917	0,340	0,330	0,913	0,330
0,646	0,899	0,318	0,341	0,920	0,341	0,330	0,913	0,330
0,646	0,899	0,318	0,341	0,903	0,341	0,332	0,917	0,332
0,646	0,899	0,318	0,341	0,920	0,341	0,332	0,910	0,332
0,659	0,899	0,324	0,343	0,906	0,343	0,332	0,906	0,332
0,722	0,920	0,722	0,354	0,906	0,354	0,333	0,920	0,333
0,727	0,934	0,727	0,364	0,924	0,364	0,336	0,910	0,336
0,936	0,889	0,341	0,621	0,899	0,305	0,680	0,899	0,334
10,884	0,840	0,523	0,625	0,899	0,307	0,716	0,896	0,321
37,314	0,816	0,551	0,697	0,899	0,342	0,724	0,896	0,324
48,003	0,809	0,503	0,704	0,896	0,315	0,912	0,889	0,332
3777,362	0,733	0,877	1,537	0,872	0,298	1,322	0,878	0,336

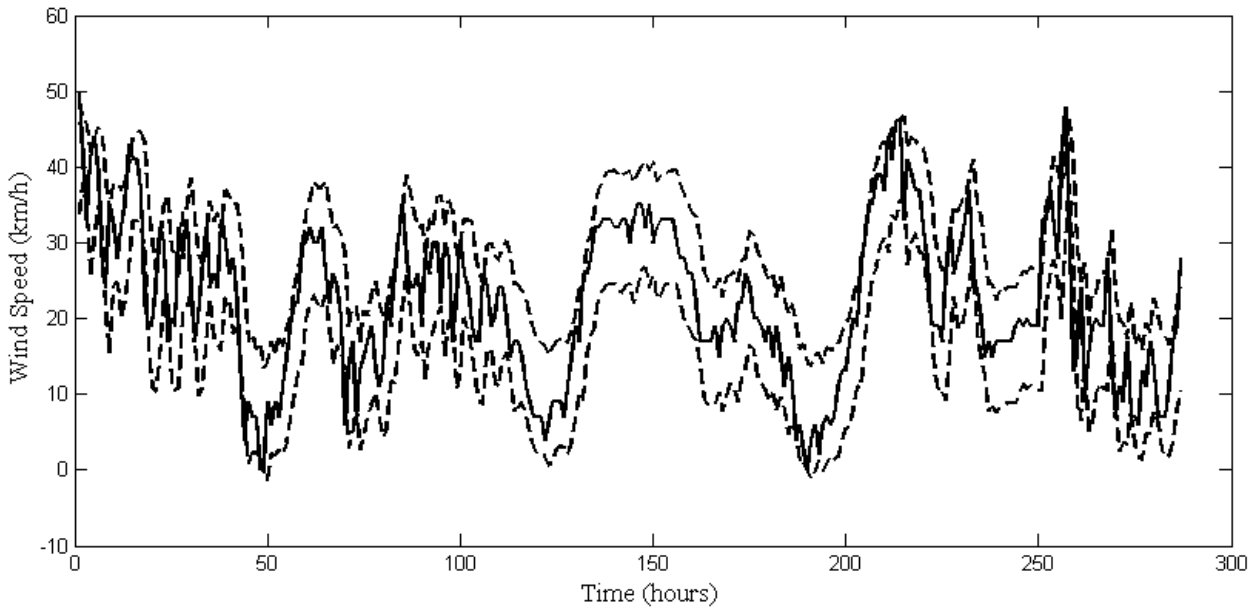


Fig. 8. Estimated PIs for 1h ahead wind speed prediction on the testing set (dashed lines), and wind speed data included in the testing set (solid line) for winter.

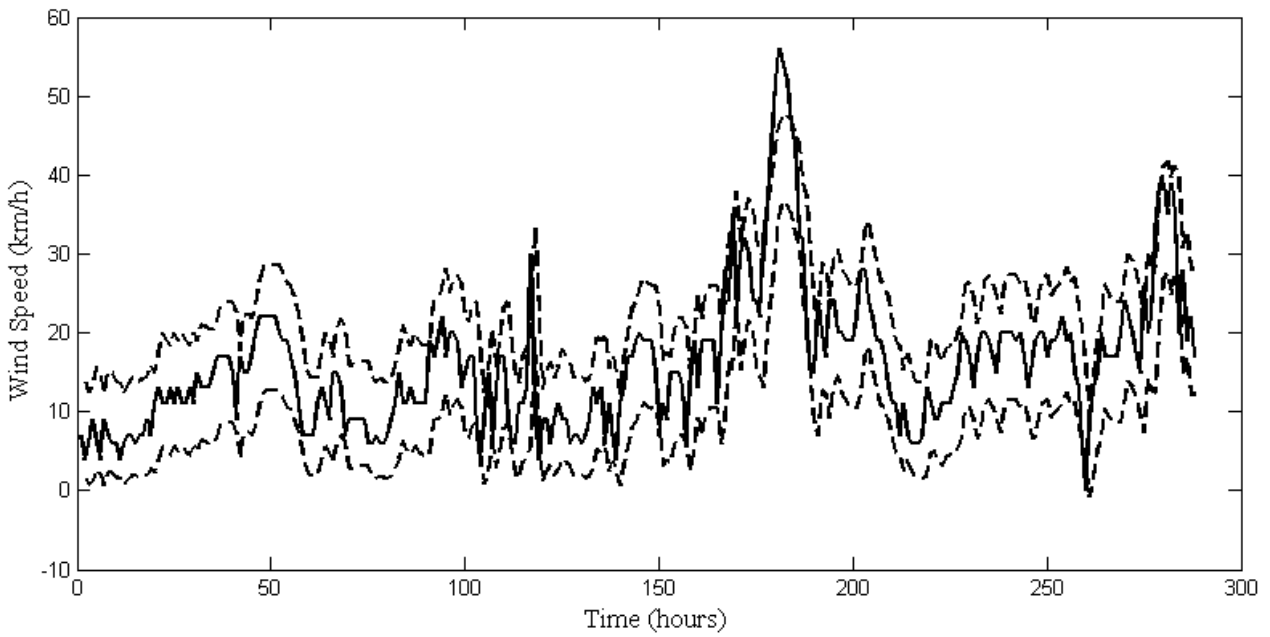
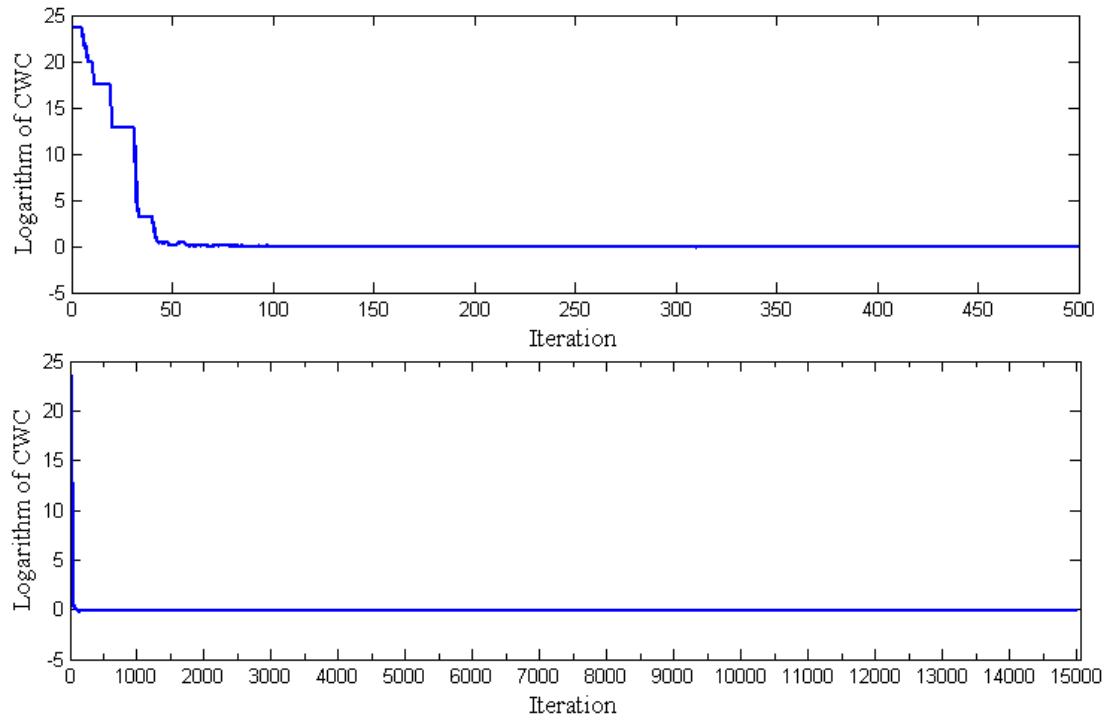
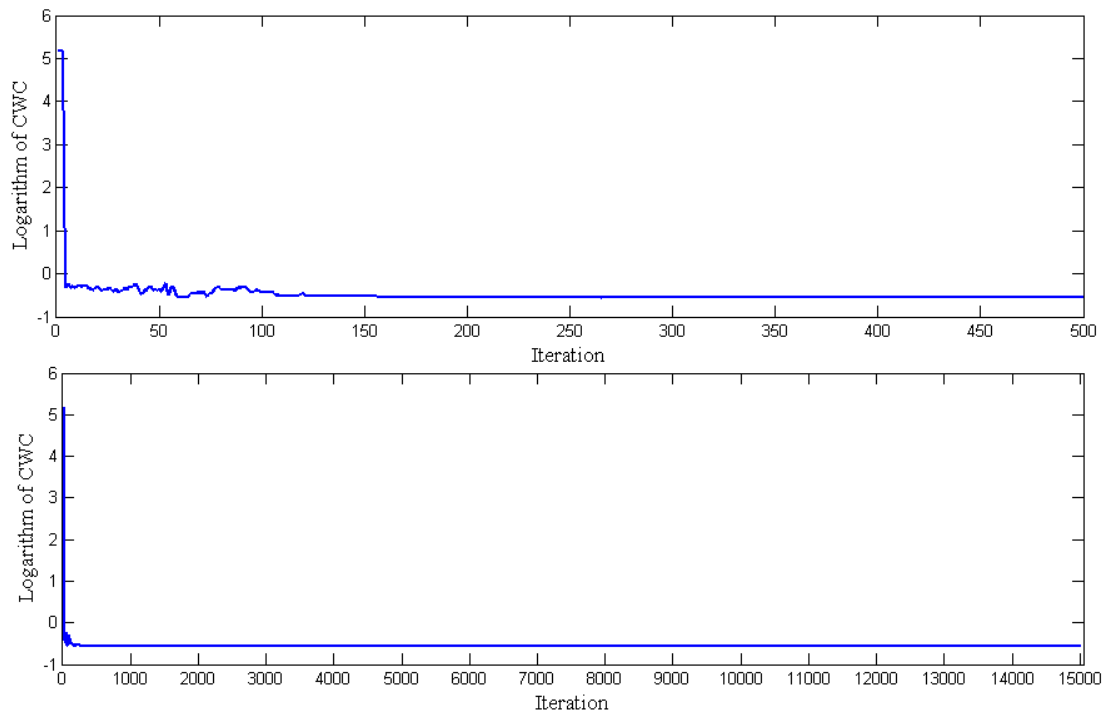


Fig. 9. Estimated PIs for 1h ahead wind speed prediction on the testing set (dashed lines), and wind speed data included in the testing set (solid line) for summer.

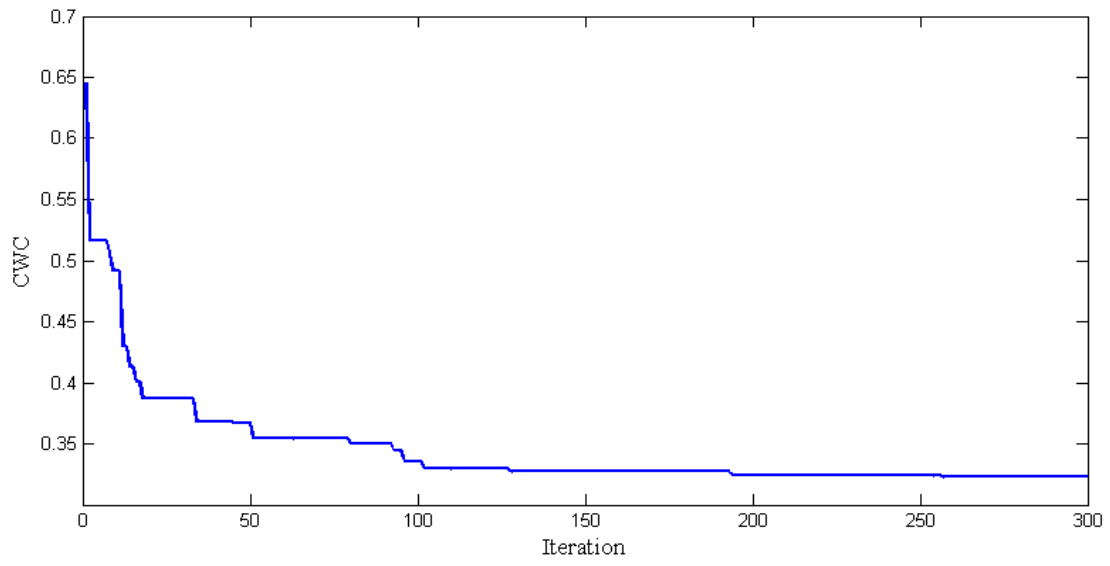


(a)

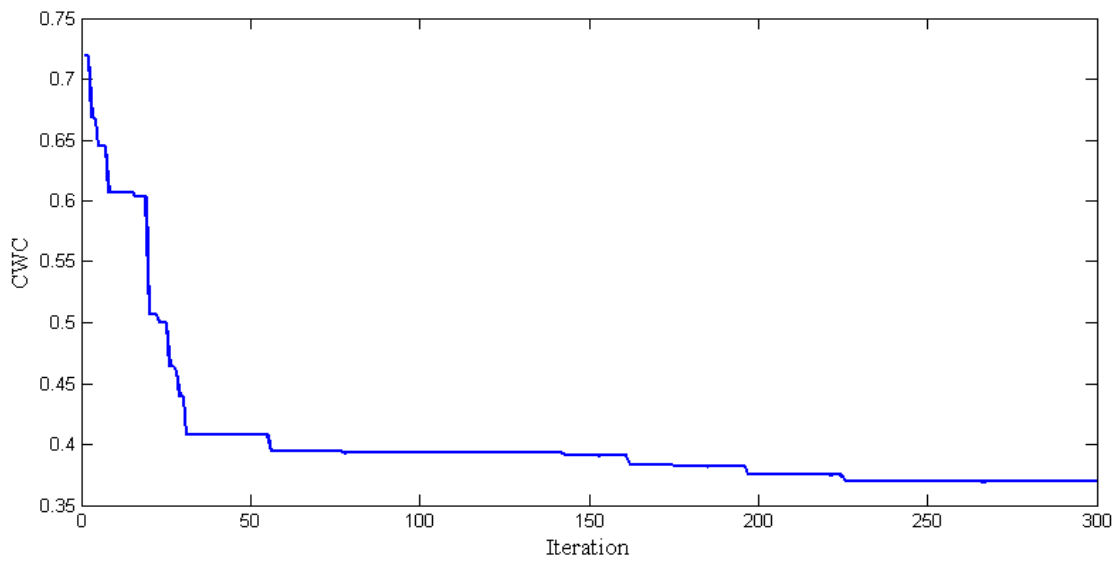


(b)

Fig. 10. Evaluation of CWC during the SOSA training algorithm: (a) winter (b) summer.

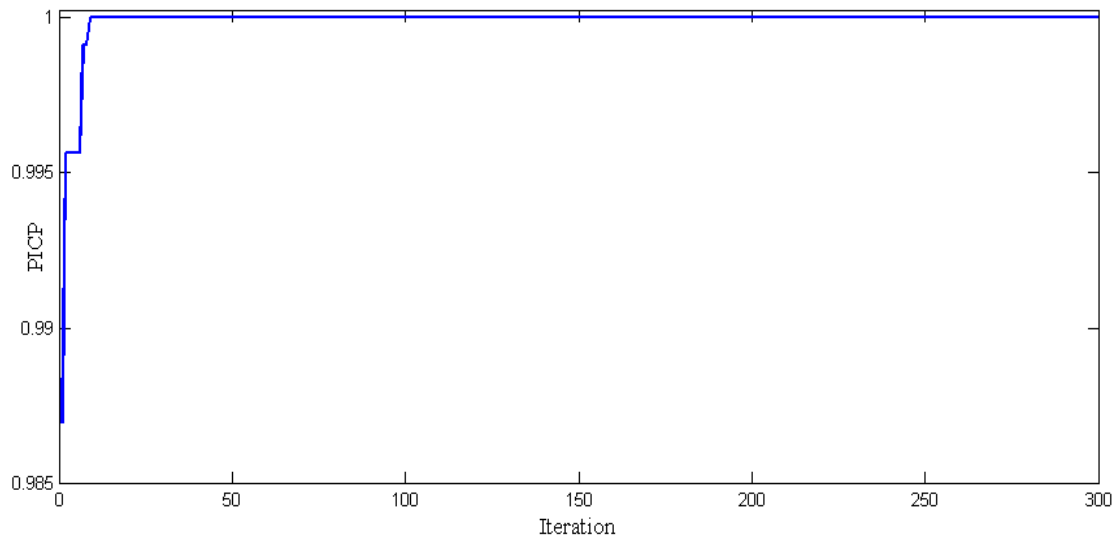


(a)

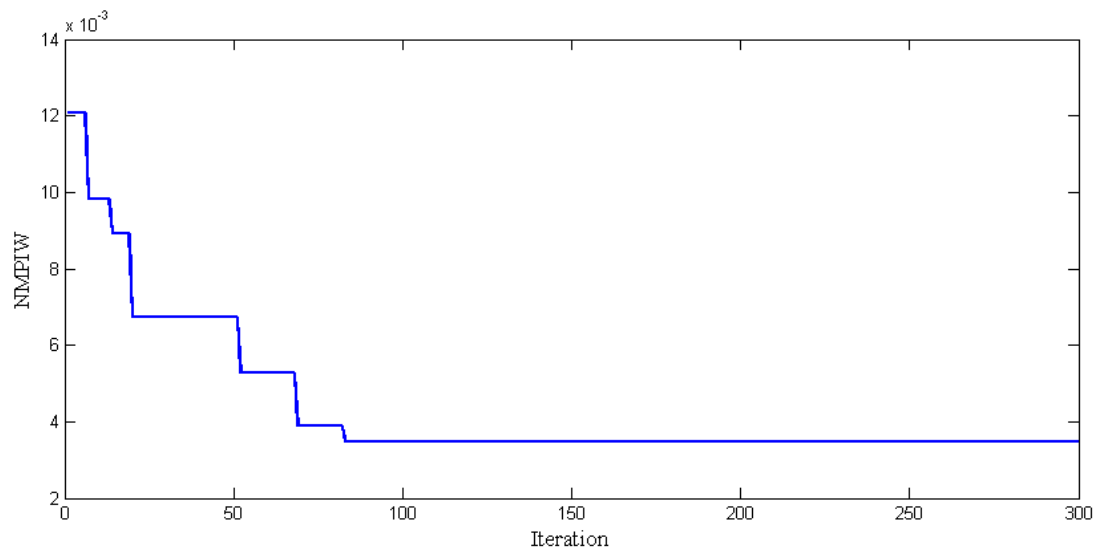


(b)

Fig. 11. Evaluation of CWC during the SOGA training algorithm: (a) winter (b) summer.

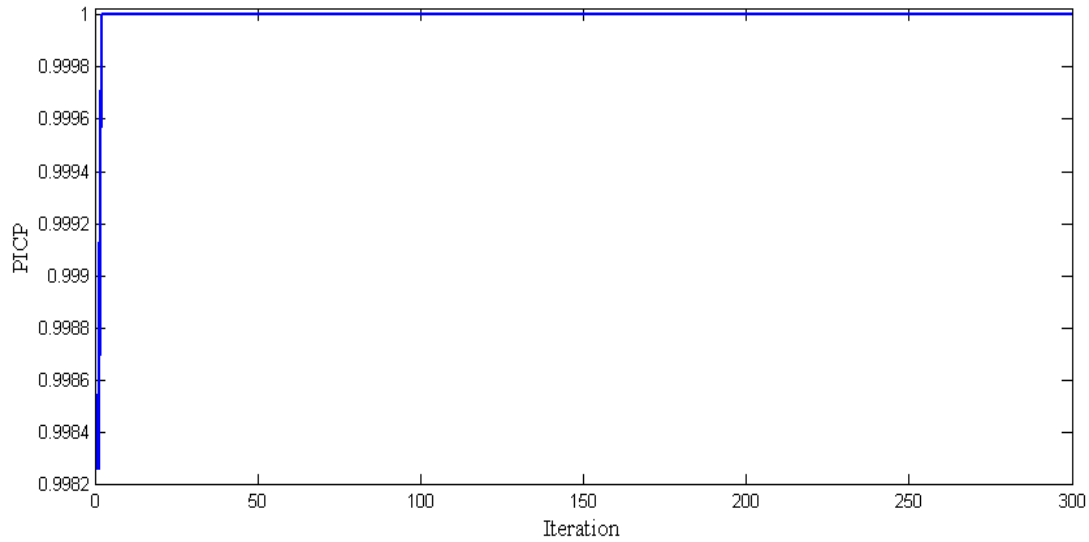


(a)

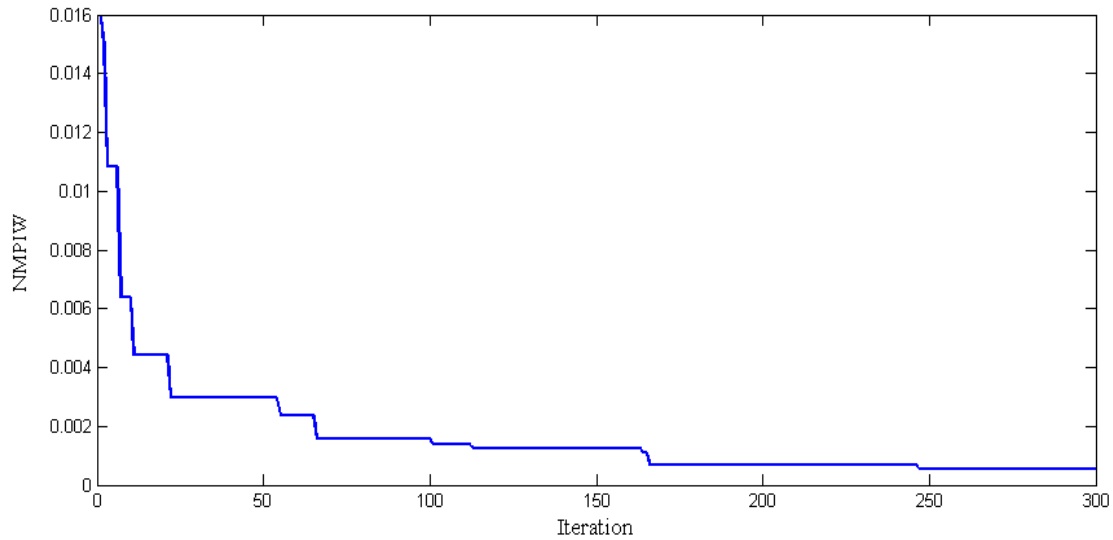


(b)

Fig. 12. Evaluation of PICP and NMPIW during the MOGA training algorithm for winter period: **(a)** PICP **(b)** NMPIW.



(a)



(b)

Fig. 13. Evaluation of PICP and NMPIW during the MOGA training algorithm for summer period: (a) PICP (b) NMPIW.

6. Conclusion

Wind speed prediction is a fundamental issue for wind power generation. The associated uncertainty needs to be properly quantified for reliable decision making in design and operation.

In this study, a method for the estimation of PIs by NN has been applied for short-term wind speed prediction. Two different time periods of historical wind speed data from Regina, Saskatchewan, have been used to demonstrate the NSGA-II capability of identifying NN weight values optimal in Pareto sense, within an original multi-objective optimization formulation of the problem of NN training. To the knowledge of the authors, this is the first study proposing such multi-objective formulation for the estimation of NN-

based PIs for wind speed prediction. The results obtained confirm the validity of the proposed approach.

The application of the non-parametric Kruskal-Wallis rank sum test to the final results obtained with SOSA, SOGA and MOGA show that the quality of the prediction intervals found with MOGA is superior to the one of the PIs found using the SOSA proposed in [12], and that it is at least comparable to the one of the PIs found using SOGA.

As for future research, the use of an ensemble of different NNs will be considered to further increase the accuracy of the predictions and the extension of the approach for prediction of wind power output will be pursued.

References

- [1] World Wind Energy Association, Half Year Report. Aug. 2011, 1-7. Online, http://www.wwindea.org/home/images/stories/publications/half_year_report_2011_wwea.pdf; Aug. 2011 [Accessed on May 2012].
- [2] The European Wind Energy Association, Wind in Power 2011 European Statistics. Online, http://www.ewea.org/fileadmin/ewea_documents/documents/publications/statistics/Stats_2011.pdf; Feb. 2012 [Accessed on May 2012].
- [3] R. G. Kavasseri, K. Seetharaman, Day-ahead wind speed forecasting using f-ARIMA models, *Renewable Energy*. 34 (2009) 1388-1393.
- [4] X. Wang, P. Guo, X. Huang, A review of wind power forecasting models, *Energy Procedia*. 12 (2011) 770-778.
- [5] M. Lei, L. Shiyuan, J. Chuanwen, L. Hongling, Z. Yan, A review on the forecasting of wind speed and generated power, *Renewable and Sustainable Energy Reviews*. 13 (2009) 915-920.
- [6] R.S. Tarade, P. K. Katti, A comparative analysis for wind speed prediction, *Proceedings of International Conference on Energy, Automation and Signal, Orissa India*, Dec. 2011, pp. 556-561.
- [7] A. M. Foley, P. G. Leahy, A. Marvuglia, E. J. McKeogh, Current methods and advances in forecasting of wind power generation, *Renewable Energy*. 37 (2012) 1-8.
- [8] W. Zhang, J. Wang, J. Wang, Z. Zhao, M. Tian, Short-term wind speed forecasting based on a hybrid model, *Applied Soft Computing*. 13 (2013) 3225-3233.
- [9] M. C. Alexiadis, P. S. Dokopoulos, H. S. Sahsamanoglou, Wind speed and power forecasting based on spatial correlation models, *IEEE Trans. Energy Convers.* 14 (1999) 836-842.
- [10] I. G. Damousis, M. C. Alexiadis, J. B. Theocharis, P. S. Dokopoulos, A fuzzy model for wind speed prediction and power generation in wind parks using spatial correlation, *IEEE Trans. Energy Convers.* 19 (2004) 352-361.
- [11] A. Khosravi, S. Nahavandi, D. Creighton, A. F. Atiya, Comprehensive review of neural network-based prediction intervals and new advances, *IEEE Transactions on Neural Networks*. 22 (2011) 1341-1356.
- [12] A. Khosravi, S. Nahavandi, D. Creighton, A. F. Atiya, Lower upper bound estimation method for construction of neural network-based prediction intervals, *IEEE Transactions on Neural Networks*. 22 (2011) 337-346.
- [13] A. Khosravi, S. Nahavandi, D. Creighton, A prediction interval-based approach to determine optimal structures of neural network metamodels, *Expert Systems with Applications*. 37 (2010) 2377-2387.
- [14] K. Deb, A. Pratap, S. Agarwal, T. Meyarivan, A fast and elitist multi-objective genetic algorithm: NSGA-II, *IEEE Transactions on Evolutionary Computation*. 6 (2002) 182-197.
- [15] R. Ak, Y. Li, E. Zio, Estimation of prediction intervals of neural network models by a multi-objective genetic algorithm, *Proceedings of Flins 2012, Istanbul*, Aug. 2012, pp. 1036-1041.
- [16] Website: http://www.weatheroffice.gc.ca/canada_e.html, (Dec., 2012).
- [17] E. Zio, A study of bootstrap method for estimating the accuracy of artificial NNs in predicting nuclear transient processes, *IEEE Transactions on Nuclear Science*. 53 (2006) 1460-1478.
- [18] L. Yang, T. Kavli, M. Carlin, S. Clausen, P. F. M. de Groot, An evaluation of confidence bound estimation methods for neural networks, *Proceedings of ESIT 2000, Sep. 2000, Aachen, Germany*, pp. 322-329.
- [19] G. Notton, C. Paoli, L. Ivanova, S. Vasileva, M. L. Nivet, Neural network approach to estimate 10-min solar global irradiation values on tilted planes, *Renewable Energy*, 50 (2013) 576-584.
- [20] Q. Zhou, J. Davidson, A. A. Fouad, Application of artificial neural networks in power system security and vulnerability assessment, *IEEE Transactions on Power Systems*. 9 (1994) 525-532.
- [21] J. M. Nazzal, I. M. El-Emam, S. A. Najim, Multilayer perceptron neural network (MLPs) for analyzing the properties of Jordan oil shale, *World Applied Sciences Journal*. 5 (2008) 546-552.
- [22] S. A. Kalogirou, Artificial neural networks in renewable energy systems applications: A review, *Renewable and Sustainable Energy Reviews*. 5 (2001) 373-401.
- [23] N. N. El-Emam, R. H. Al-Rabeh, An intelligent computing technique for fluid flow problems using hybrid adaptive neural network and genetic algorithm, *Applied Soft Computing*. 11 (2011) 3283-3296.
- [24] R. Dybowski, S. J. Roberts, Confidence intervals and prediction intervals for feed-forward neural networks, in: R. Dybowski, V. Gant (Eds.), *Clinical Applications of Artificial Neural Networks*, Cambridge University Press, 2011, pp. 298-326.
- [25] D. J. C. MacKay, Bayesian interpolation, *Neural Computation*. 4 (1992) 415-447.
- [26] C. P. I. J. Van Hinsbergen, J. W. C. Van Lint, H. J. Van Zuylen, Bayesian committee of neural networks to predict travel times with confidence intervals, *Transportation Research Part C*, 17 (2009) 498-509.
- [27] D. A. Nix, A. S. Weigend, Estimating the mean and the variance of the target probability distribution, *Proceedings of IEEE Int. Con. Neural Netw. World Congr. Comput. Intell., Orlando, FL., Jun. 27 - Jul. 2, 1994*, pp. 55-60.
- [28] R. W. Johnson, An introduction to the bootstrap, *Teaching Statistics*, 23 (2001) 49-54.
- [29] Y. Sawaragi, H. Nakayama, T. Tanino, *Theory of Multi-objective Optimization*, Orlando, FL, Academic Press Inc., 1985.
- [30] A. Konak, D. W. Coit, A. E. Smith, Multi-objective optimization using genetic algorithms: a tutorial, *Reliability Engineering and System Safety*. 91 (2006) 992-1007.
- [31] R. Furtuna, S. Curteanu, F. Leon, Multi-objective optimization of a stacked neural network using an evolutionary hyper-heuristic, *Applied Soft Computing*. 12 (2012) 133-144.
- [32] E. Zitzler, L. Thiele, Multi-objective evolutionary algorithms: a comparative case study and the strength Pareto approach, *IEEE Transactions on Evolutionary Computation*, 3 (1999) 257-271.
- [33] N. Sirinivas, K. Deb, Multi-objective optimization using non-dominated sorting in genetic algorithms, *Journal of Evolutionary Computation*. 2 (1994) 221-248.
- [34] H. Mühlenbein, D. Schlierkamp-Voosen, Predictive models for the breeder genetic algorithm: I. continuous parameter optimization, *Evolutionary Computation*. 1 (1993) 25-49.
- [35] M. Bessaou, P. Siarry, A genetic algorithm with real-value coding to optimize multimodal continuous functions, *Structural and Multidisciplinary Optimization*. 23 (2001) 63-74.
- [36] M. Srinivas, L. M. Patnaik, Adaptive Probabilities of crossover and mutation in genetic algorithms, *IEEE Transactions on Systems, Man and Cybernetics*. 24 (1994) 656-667.
- [37] Z. Michalewicz, *Genetic Algorithms + Data Structures = Evolution Programs*, Springer-Verlag, New York, 1992.
- [38] Canadian Wind Energy Association (CanWEA), Media Kit 2012. Online, http://www.canwea.ca/pdf/windsight/CanWEA_MediaKit.pdf; 2012 [Accessed on May 2012].
- [39] SaskPower Annual Report 2011. Online, http://www.saskpower.com/news_publications/assets/annual_reports/2011_skpower_annual_report.pdf; 2011 [Accessed on May 2012].
- [40] J.L. Rodgers, W.A. Nicewander, Thirteen ways to look at the correlation coefficient, *The American Statistician*. 42 (1988) 59-66.
- [41] M. Hollander, D. A. Wolfe, *Nonparametric Statistical Methods*, John Wiley & Sons, New York, 1973.
- [42] T. Hastie, R. Tibshirani, J. Friedman, *The elements of Statistical Learning: Data Mining, Inference and Prediction*, second ed., Springer, 2008.
- [43] R. Karki, P. Hu, R. Billinton, A simplified wind power generation model for reliability evaluation, *IEEE Transactions on Energy Conversion*. 21 (2006) 533-540.
- [44] N.L. Buccola, T.M. Wood, Empirical models of wind conditions on upper Klamath lake, Oregon, *Scientific Investigations Report 2010-5201*, Online, <http://pubs.usgs.gov/sir/2010/5201/pdf/sir20105201.pdf>; 2010, [Accessed on May 2012].
- [45] G. E. P. Box, G. M. Jenkins, G. C. Reinsel, *Time Series Analysis, Forecasting and Control*, fourth ed., Wiley, 2008.
- [46] E. Zio, P. Baraldi, and N. Pedroni, Optimal power system generation scheduling by multi-objective genetic algorithms with preferences, *Reliability Engineering and System Safety*. 94 (2009) 432-444.
- [47] S. Bandyopadhyay, S. Saha, U. Maulik, K. Deb, A Simulated annealing-based multi-objective optimization algorithm: AMOSA. *IEEE Transactions on Evolutionary Computation*. 12 (2008) 269-283.
- [48] E. L. Ulungu, J. Teghem, Ch. Ost, Efficiency of interactive multi-objective simulated annealing through a case study, *Journal of the Operational Research Society*. 49 (1998) 1044-1050.
- [49] R. A. Johnson, D. W. Wichern, *Applied Multivariate Statistical Analysis*, fifth ed., Pearson Education Inc., 2002.
- [50] D. F. Bauer, Constructing confidence sets using rank statistics, *Journal of the American Statistical Association*. 67 (1972) 687-690.



Ronay Ak received the B.Sc. degree in mathematical engineering from Yildiz Technical University, Istanbul, Turkey, in 2004 and the M.Sc. degree in industrial engineering from Istanbul Technical University, Istanbul, Turkey in 2009. She is currently pursuing the Ph.D. degree at Chair on Systems Science and the Energetic Challenge, European Foundation for New Energy-Électricité de France (EDF), École Centrale

Paris (ECP) and École Supérieure d'Électricité (SUPELEC), France, since March 2011. Her research interests include uncertainty quantification, prediction methods, artificial intelligence, reliability analysis of wind-integrated power networks and optimization heuristics.



Yanfu Li is an Assistant Professor at Ecole Centrale Paris (ECP) & Ecole Supérieure d'Electricite (SUPELEC), Paris, France. Dr. Li completed his PhD research in 2009 at National University of Singapore, and went to the University of Tennessee as a research associate. His current research interests include reliability modeling, uncertainty analysis, evolutionary computing, and Monte Carlo simulation. He is the

author of more than 30 publications, all in refereed international journals, conferences, and books. He is an invited reviewer of over 10 international journals.



Valeria Vitelli received the B. Sc. and the M. Sc. degrees in mathematical engineering from Politecnico di Milano, Milan, Italy, in 2006 and 2008, respectively. She received the Ph.D. degree in Mathematical Models and Methods for Engineering, with a focus on statistical models for classification of high-dimensional data, in May 2012. She worked as a postdoc researcher within the Chair on Systems Science and the Energetic

Challenge, European Foundation for New Energy- Électricité de France (EDF), École Centrale Paris (ECP) and École Supérieure d'Électricité (SUPELEC), France, from February 2012 to May 2013.



Enrico Zio received the Ph.D. degree in nuclear engineering from Politecnico di Milano and MIT in 1995 and 1998, respectively. He is currently Director of the Chair on Systems Science and the Energetic Challenge, European Foundation for New Energy-Électricité de France (EDF), at École Centrale Paris (ECP) and École Supérieure d'Électricité (SUPELEC) and full professor at Politecnico di Milano. His research

focuses on the characterization and modeling of the failure/repair/maintenance behavior of components, complex systems and their reliability, availability, maintainability, prognostics, safety, vulnerability and security, advanced Monte Carlo simulation methods, soft computing techniques and optimization heuristics.